Turkish Journal of Electrical Engineering & Computer Sciences

http://journals.tubitak.gov.tr/elektrik/

Research Article

Turk J Elec Eng & Comp Sci
(2015) 23: 1958 – 1980

doi: elk-1404-226

Stability preservation and power management in autonomous microgrids using adaptive nonlinear droop scheme

Sara NOUROLLAH*, Abolfazl PIRAYESH, Poria ASTERO
Department of Electrical and Computer Engineering, Shahid Beheshti University, Tehran, Iran

Received: 13.04.2014 • **Accepted/Published Online:** 14.07.2015 • **Final Version:** 30.11.2015

Abstract: This paper proposes sharing active and reactive power in autonomous voltage source inverter (VSI)-based microgrids with no physical communication links. In decentralized VSI-based microgrids, when the demand or generation changes, the output voltage of distributed generation units and the frequency of the system will also change. This study presents a novel adaptive nonlinear droop (ANLD) scheme for preserving network stability, improving the system's dynamics, and controlling power sharing in multibus microgrids in a decentralized manner. Subcontrollers are modeled in a state space and combined together so that a complete dynamic model of the network can be developed. Note that controller coefficients are optimized to improve small-signal stability and to obtain a good operating point. To this end, an optimization problem is formulated and solved using the particle swarm optimization method. For the purposes of comparison, the proposed ANLD method and three other schemes are applied to two case studies: a 5-bus microgrid and a modified 37-bus IEEE microgrid. The stability margin analysis and time response simulations prove that the proposed algorithm performs much better and can be applied to large-scale microgrids.

Key words: Autonomous microgrid, droop control, load sharing, small-signal dynamics, voltage source inverter model

1. Introduction

Nowadays there is an increasing demand for energy in the form of stand-alone and small networks. There are several issues about supplying energy and launching such networks: resource type, system stabilization, power sharing, prevention of voltage collapse, and so on.

A microgrid is a part of a power distribution system [1,2] that constitutes a localized group of distributed generation (DG) units and loads that are usually interconnected and synchronous with the conventional distribution grid [2–4]. Microgrids can be designed as smart networks that turn the traditional process of generation, transmission, and distribution into an intelligent distribution scheme, taking advantage of new concepts and technologies. Microgrids are intended to increase reliability, improve power quality, reduce costs of generation and transmission, and employ renewable recourses in lieu of fuel sources [3–6]. In addition, the presence of controllers in a microgrid reduces circulating reactive power, voltage droop, and frequency variation; improves active and reactive power sharing; and increases stability margin in transient and steady states. Microgrids have two different modes. In normal situations, they are connected to the network. However, when the power quality of the upstream network is not good, they disconnect from the network and work in autonomous mode. A common problem of microgrids in islanded mode is that they cannot live up to expectations due to a surge in the demand for power or because some of the resources go out of service for maintenance or replacement.

*Correspondence: s_nourollah@sbu.ac.ir

In autonomous microgrids, all DG units must share the load, regulate the system voltage, keep the network frequency at nominal value, and prevent circulating current [7,8]. This calls for some controllers to take charge of the situation.

For controlling the VSI-based microgrid, two techniques are seen in the previous studies. The first one is based on a communication link, such as in [6,9–11]. In these studies, the master-slave scheme is applied. Pecas Lopes et al. [11] studied autonomous microgrids by selecting some DG as the multiple-master and also selecting a DG as single-master, and they finally concluded that both methods ensure system stability under different load conditions. However, physical communication links decrease the system reliability, and in large-scale systems this is impractical and costly.

The second idea is the droop method; this approach solves the presented communication link problems. The control schemes proposed in [11–16] are based on conventional droop. However, the conventional technique could not preserve the network frequency and voltage at their nominal values.

In low-voltage grids, line characteristics are resistive. Hence, active power and voltage are linked together. A phase difference of voltage between the sources also causes reactive power flow. For this reason, some studies [17–19] proposed (P/V) and (Q/f) droops and called them "opposite droops". Using opposite droop, the voltage can be controlled directly. However, voltage deviations remain in the system [19].

To eliminate the frequency and voltage deviations, many studies [20–26] presented new and modified (P/f) and (Q/v) droops. Vasquez et al. [22] presented adaptive phase and voltage droops, where both of them depend on active and reactive power. In [24], for compensating voltage unbalance, positive and negative sequences of parameters were used in droop equations. Another study [25] proved that voltage and frequency droop equations depend on $\frac{dQ}{dt}$ and $\frac{dP}{dt}$ terms, respectively, and that it increases stability margin compared to conventional droop. Some studies, such as [21,26,27], researched the improvement of the system voltage only.

This manuscript proposes a novel adaptive nonlinear droop characteristic for not only preserving system stability but also for proper sharing of active and reactive loads, decreasing voltage and frequency deviations, and increasing system reliability. Performance and authenticity of the proposed idea will be demonstrated by theoretical analysis and simulation and it will be proved that the proposed method is better than other strategies proposed by previous studies.

The remainder of this paper is organized as follows. Section 2 gives a description of the structure of a microgrid, which includes DG units, loads, and lines, and presents the internal structure of VSI-based DG units. Also in this section, the issue of how to solve network equations to obtain operating point and time response of the system is discussed. In Section 3, a novel adaptive nonlinear droop (ANLD) method of active and reactive power control for VSI-based microgrids in autonomous mode is proposed. Section 4 deals with the optimization of the coefficients of the ANLD scheme in order to make sure the system gives a desirable and optimized response. The configuration of test cases and simulation results are reported in Section 5, followed by the conclusion in Section 6.

2. Microgrid structure

A microgrid has three main sections: DG units, loads, and lines. In a distribution network, the lines are resistive, and also, in VSI-based microgrids, the dynamics of inverters are very fast [28]. Hence, the loads and lines must be modeled in dynamic mode. In this study, the dynamic models of the loads and lines are based on the equations of [12].

2.1. VSI-based DG unit

The control structure of the DG unit, based on the method proposed in [12], is composed of the following sections: a power controller (PC), voltage controller (VC), current controller (CC), and filtering system (FS). This structure is demonstrated in Figure 1. The PC is the most important control section.

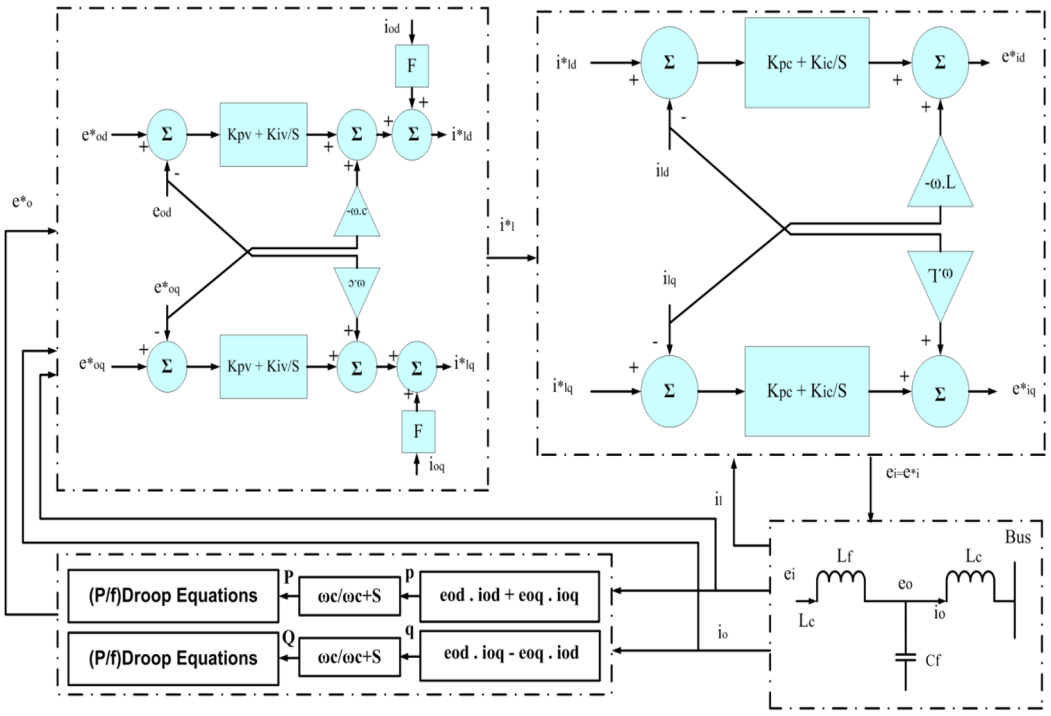

Figure 1. Voltage source inverter block diagram in DG unit.

In a decentralized microgrid, each controller in the DG must respond rapidly to network changes without receiving data from loads and other DGs [2]. Hence, VSIs (DGs) must be equipped with the (P/f) and (Q/v) droop controller. Using this scheme, the DGs share a common active load together, by dropping the frequency of their output voltage. Also, for sharing the common reactive load, they drop their output voltage magnitude despite increasing output reactive power [2]. This idea is taken from power sharing control of traditional synchronous generators [29].

The PC regulates the frequency and magnitude of the output voltage of the DG by the droop characteristics according to measured active and reactive power in the DG. In PC implementation, the measured active and reactive power is passed through a low-pass filter. This filter eliminates variations of power and voltage, creates delay, and prevents the VC and the CC from interfering with the PC [25]. Eq. (1) expresses the measured active and reactive power in the local rotating frame.

$$\begin{cases} \tilde{p} = e_{od}.i_{od} + e_{oq}.i_{oq} \\ \tilde{q} = e_{od}.i_{oq} - e_{oq}.i_{od} \end{cases} \tag{1}$$

Here, e_{od} and e_{oq} are the direct and quadratic components of measured output voltage of the DG unit, respectively, and i_{od} and i_{oq} are the direct and quadratic components of measured output current of the DG

unit, respectively. Eq. (2) shows low-pass filter equations.

$$\begin{cases} P = \frac{\omega_c}{s+\omega_c}\tilde{p} \\ Q = \frac{\omega_c}{s+\omega_c}\tilde{q} \end{cases} \tag{2}$$

Here, ω_c is the cut-off frequency, and P and Q are the state variables of average active and reactive power, respectively. If P and Q are put in conventional (P/f) and (Q/V) droop equations, respectively, the reference magnitude (e^*_{od},e^*_{oq}) and phase (δ) of the output voltage of the DG unit are calculated according to Eqs. (3) and (4).

$$\begin{cases} e^*_{od} = |e_{0j}| - n_1.Q \\ e^*_{oq} = 0 \end{cases} \tag{3}$$

$$\begin{cases} \omega = \omega_n - m_1.P \\ \epsilon = \omega_n.t + \delta \\ \omega = \epsilon \\ \delta = -m_1.P \end{cases} \tag{4}$$

Here, $|e_{0j}|$ and ω_n are nominal voltage and frequency in the local frame, respectively. In addition, m_1 and n_1 are coefficients of frequency and voltage droops, respectively. Coefficients m_1 and n_1 are solvable in different ways. A common approach is using Eq. (5).

$$\begin{cases} m_1 = \frac{\omega_{max} - \omega_{min}}{P_{max}} \\ n_1 = \frac{e_{od,max} - e_{od,min}}{Q_{max}} \end{cases} \tag{5}$$

In Eqs. (3) and (4) above, the phase and the amplitude of voltage are calculated in the local rotating frame of the inverter. In order to transfer this local frame to the reference frame, the difference in angle between the two frames (ϑ) needs to be calculated, and this is accomplished using Eq. (6).

$$\vartheta = \int (\omega - \omega_{com}) \tag{6}$$

The PC needs (Q/V) and (P/f) droops to be designed. In Section 3, novel droop equations will be proposed and analyzed.

The VC and CC controllers use the proportion-integrated (PI) controller and the feedforward scheme for eliminating the output voltage error and the input current error of the FS, respectively. Also, the FS rejects high-frequency deviations [12].

2.2. Network equations solution

It is a known fact that in autonomous microgrids, the frequency of each DG unit varies around the nominal frequency depending on load conditions and droop characteristics. These variations cause the rotating frame of each DG unit to rotate at a different speed. Figure 2 shows the rotating frame of the ith DG (d_i–q_i), that of

the jth DG $(d_j - q_j)$, and the reference rotating frame $(D-Q)$ at frequencies ω_i, ω_j, and ω_{com}, respectively. In order to transfer the rotating frame of the ith DG to the reference frame, Eq. (7) can be used.

$$[f_{DQ}] = [TM_i]\,[f_{dqi}] \tag{7}$$

Here $[TM_i]$ is the transfer matrix of the ith DG, which is expressed using Eq. (8).

$$[TM_i] = \begin{bmatrix} \cos(\vartheta_i) & -\sin(\vartheta_i) \\ \sin(\vartheta_i) & \cos(\vartheta_i) \end{bmatrix} \tag{8}$$

Here, ϑ_i is the difference in angles between the reference frame and the ith frame. In a microgrid, if all DG resources are VSI-based, then one of them must be regarded as the reference, with its ϑ being zero. In this paper, if a parameter is in the reference frame, then it is written using capital letters; otherwise, lowercase letters will be used.

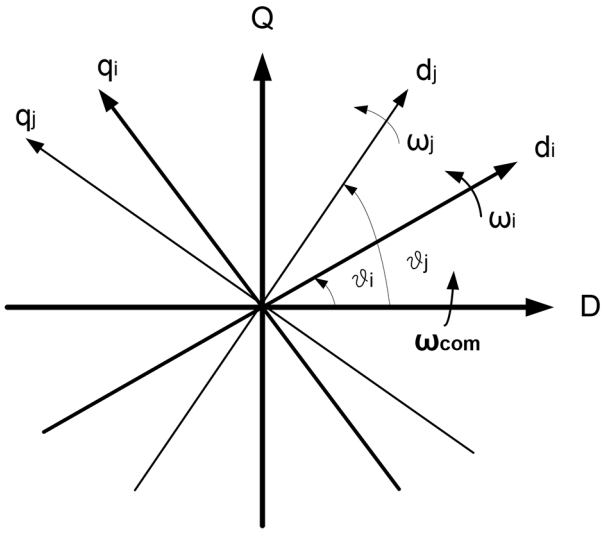

Figure 2. Rotating frames of the ith DG and the jth DG as well as the reference rotating frame.

In the n-bus system, there are 2n unknown variables [12]. To solve these state equations, 2n equations are needed, which are obtained using the KCL in each bus, as in Eq. (9). Indeed, using Eq. (9), all variables are linked together.

$$\begin{cases} \sum I_{Dload,line,andDG} = 0 \\ \sum I_{Qload,line,andDG} = 0 \end{cases} \tag{9}$$

Finally, all network equations consist of some state equations that model the network and some algebraic equations that connect the network elements together. Generally, all these equations can be written as in Eq. (10) below.

$$\begin{cases} \dot{x} = H(x,y,z) \\ 0 = E(x,y,z) \end{cases} \tag{10}$$

Here, x is a dynamic-state variable such as the current of dynamic loads, y is an algebraic state variable such as the amplitude and phase of voltage of the DG bus, and z is a miscellaneous parameter. H and E

represent dynamic and algebraic equations, respectively. The process of formulating and solving the state and algebraic equations is depicted in Figure 3 [12].

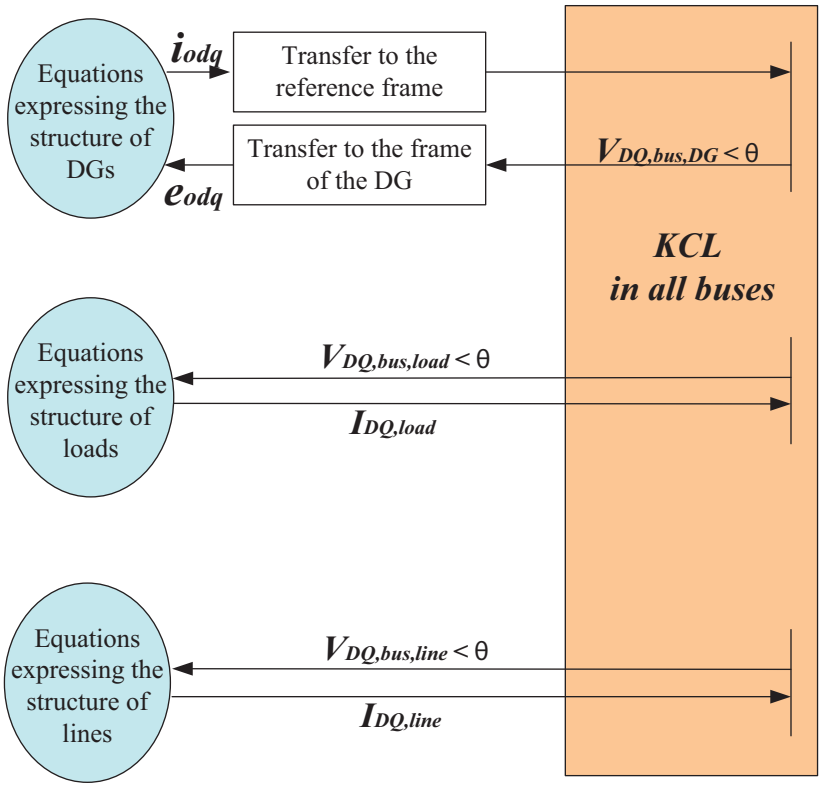

Figure 3. The block diagram of developing the complete state space model of the microgrid.

In the steady state, the system is stable, and therefore all variables are constant ($x' = 0$). Thus:

$$\begin{cases} H(x,y,z) = 0 \\ E(x,y,z) = 0 \end{cases} \tag{11}$$

For obtaining the operating point, Eq. (11) must be solved. In this study Newton's method is used [30].

Eigenvalues are the roots of the characteristic equation of the system state matrix (A). To obtain the state matrix, the Jacobean matrix (J) must first be calculated using Eq. (12).

$$J = \begin{bmatrix} \frac{dH}{dx} & \frac{\partial H}{\partial y} \\ \frac{dE}{dx} & \frac{dE}{dy} \end{bmatrix} = \begin{bmatrix} H_x & H_y \\ E_x & E_y \end{bmatrix} \tag{12}$$

Now the state matrix can be expressed as in Eq. (13).

$$A(x,y,z) = \{H_x\} - H_y E_y^{-1} E_x \tag{13}$$

Also, obtaining the time response of the system requires Eq. (10) to be solved using the algorithm proposed in [31].

3. Proposed ANLD controller

With the aim of increasing the stability margin and reliability of the system, following variations in the load, eliminating circulating reactive power between DG units, and reducing perturbations of voltage and frequency, the following proponed ANLD structure for the PC is developed in two subsections.

3.1. The proposed reactive power control technique

3.1.1. The first theory

Figure 4 is the single-line diagram of the microgrid under consideration, as in [12]. The output current of the jth DG in this microgrid is written as in Eq. (14).

$$I_j<\theta_j=\frac{\{E_j<\delta_j\}-\{|V_j|<\alpha_j\}}{z_j} \tag{14}$$

If DG_1 is defined as a reference, then $\alpha_1=0$ and the output current and power of this DG can be presented as in Eqs. (15) and (16), respectively.

$$I_1<\theta_1=\frac{\{E_1\cos\delta_1-|V_1|\}+j\{E_1\sin\delta_1\}}{z_1} \tag{15}$$

$$\begin{cases} P_1=\frac{r_1.E_1^2+|V_1|.E_1.(r_1.\cos\delta_1+x_1.\sin\delta_1)}{r_1^2+x_1^2} \\ Q_1=\frac{x_1.E_1^2+|V_1|.E_1.(r_1.\sin\delta_1-x_1.\cos\delta_1)}{r_1^2+x_1^2} \end{cases} \tag{16}$$

Eq. (17) can be obtained from Eq. (16).

$$Q_1=\frac{r_1.P_1}{x_1}+\frac{E_1^2-|V_1|.E_1.\cos\delta_1}{x_1} \tag{17}$$

It can be concluded that P_1 and Q_1 are linked together and that the relationship between V_1 and Q_1 is nonlinear. On the other hand, according to [25], the voltage droop characteristic depends on the term $\frac{dQ}{dt}$. Hence, in this paper, the nonlinear function F_1 is proposed for the (Q/v) droop according to Eq. (18).

$$F_1=\frac{dQ}{dt}+\frac{dP}{dt} \tag{18}$$

3.1.2. The second theory

In Figure 4, the voltage of the jth bus is computed using Eq. (19).

$$|V_j|<\alpha_j=E_j<\delta_j-Z_jI_j<\theta_j \tag{19}$$

Here, $I_j<\theta_j$ and $E_j<\delta_j$ are the output current and voltage of the jth DG, respectively. Z_j is the impedance of the jth line. Eq. (19) can be expanded into Eqs. (20) and (21) as shown below.

$$|V_j|<\alpha_j=\{E_j.\cos(\delta_j)-r_jI_j.\cos(\theta_j)-x_jI_j.\sin(\theta_j)\}+j\{E_j.\sin(\delta_j)+r_jI_j.\sin(\theta_j)-x_jI_j.cos(\theta_j)\} \tag{20}$$

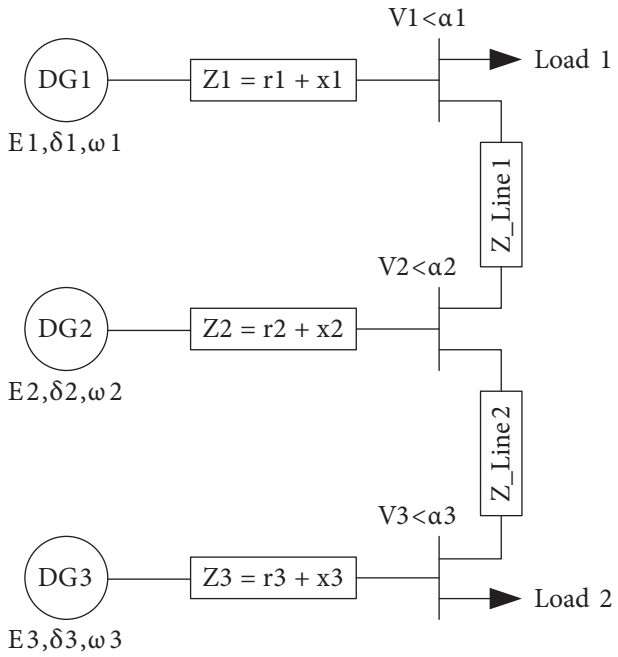

Figure 4. Single-line diagram of the microgrid under investigation.

$$|V_j| = \left\{E_j^2 + r_j^2 I_j^2 + x_j^2 I_j^2 - 2E_j r_j I_j . \cos(\delta_j + \theta_j) - 2E_j x_j I_j . \sin(\delta_j + \theta_j)\right\}^{1/2} \tag{21}$$

Assuming that $\Gamma_j = \delta_j + \theta_j$, $\Gamma_j \cong$ and $x_j \cong$,

then $x_j^2 I_j^2 \cos^2(\Gamma_j) \cong 0$, $r_j^2 I_j^2 \sin^2(\Gamma_j) \cong 0$ and $2 r_j x_j I_j^2 . \sin(\Gamma_j) . \cos(\Gamma_j) \cong 0$.

Thus, Eq. (21) can be expressed as Eq. (22).

$$|v_j| = \left\{E_j^2 + r_j^2 I_j^2 \cos^2(\Gamma_j) + 2 r_j x_j I_j^2 \sin(\Gamma_j) . \cos(\Gamma_j) + x_j^2 I_j^2 \sin^2(\Gamma_j) - 2E_j r_j I_j . \cos(\Gamma_j) - 2E_j x_j I_j . \sin(\Gamma_j)\right\}^{\frac{1}{2}} \tag{22}$$

Eq. (22) can be simplified as Eq. (23).

$$|V_j| = \{E_j - r_j I_j \cos(\Gamma_j) - x_j I_j \sin(\Gamma_j)\} \tag{23}$$

On the other hand, the power generated by the jth DG is calculated from Eq. (24).

$$S_j = (E_j < \delta_j)(I_j < \theta_j)^* \tag{24}$$

Eq. (25) can be obtained from Eq. (24).

$$\begin{cases} P_j = E_j I_j . \cos(\Gamma_j) \\ Q_j = E_j I_j . \sin(\Gamma_j) \end{cases} \tag{25}$$

Using Eq. (25), Eq. (23) can be rewritten as Eq. (26) below.

$$|V_j| = E_j - r_j \left(\frac{P_j}{E_j}\right) - x_j \left(\frac{Q_j}{E_j}\right) \tag{26}$$

According to Eq. (26), the voltage droop function, F_2, in each bus is expressed as Eq. (27).

$$F_2 = r_j \left(\frac{P_j}{E_j}\right) + x_j \left(\frac{Q_j}{E_j}\right) = Real\left\{\frac{\bar{Z}_j . S_j}{|E_j|}\right\} \tag{27}$$

Eq. (26) shows that voltage amplitude depends not only on the reactive power but also on the active power and series impedance (Z_j). Furthermore, Z_j gives rise to voltage droop. Hence, it is necessary that F_2 be added to the voltage droop equation in order to improve the voltage profile.

The first and second theories hold true for nonreference DGs. According to these theories, in this literature, the proposed (Q/V) droop of the jth DG is developed as in Eq. (28) instead of the conventional droop equation (Eq. (3a)). In Section 5, the validity of the scheme will be proved.

$$|V_j| = |E_{0j}| - n_{1j}\left(Q_j - Q_{0j}\right) - n_{2j}\frac{dQ_j}{dt} - n_{3j}\frac{dP_j}{dt} + Real\left\{\frac{\bar{Z}_j . S_j}{|E_{0j}|}\right\} \tag{28}$$

3.2. The proposed active power control technique

In this subsection, a novel (P/f) droop characteristic, Eq. (29), is presented and applied in the PC instead of Eq. (4a). This proposal eliminates the frequency deviations while improving the system stability and sharing the active power. Considering that [25] proposed the term $\frac{dP}{dt}$ in the (P/f) droop equation, the following equation is proposed.

$$\omega_j = \omega_{nj} - m_{1j}\left(P_j - P_{0j}\right) - m_{2j}\frac{dP_j}{dt}\left(P_j - P_{0j}\right) \tag{29}$$

In order to prove the performance and validity of Eq. (29), eigenvalues of conventional and proposed droop equations are calculated.

If $r_{j\cong 0}$ and $\delta_{j\cong 0}$ are assumed in Figure 4, Eq. (30) is obtained from Eq. (16).

$$P_j = \frac{|V_j| . E_j . \sin\delta_j}{x_j} \tag{30}$$

On the other hand, Eq. (6) above can be expressed as Eq. (31).

$$\delta_j - \delta_s = \int \left(\omega_j - \omega_s\right) . dt \tag{31}$$

Here, δ_s and ω_s are related to the reference DG unit, and δ_j and ω_j are related to DG_j, which is the nonreference DG. It should be noted that the conventional (P/f) droop mimics governor characteristics in the synchronous generator [32]. If V_j, E_j, and x_j are assumed constant, $\frac{dP_j}{dt}$ is calculated using Eq. (32).

$$\frac{dP_j}{dt} = \frac{|V_j| . E_j . \cos(\delta_j - \delta_s)}{x_j}\left(\frac{d\delta_j}{dt} - \frac{d\delta_s}{dt}\right) \tag{32}$$

Eq. (33) is presented using Eq. (4a) and Eq. (31),

$$\frac{dP_j}{dt} = A . \left\{\omega_j - \omega_s\right\}, \tag{33}$$

where

$$A = \frac{|V_j|.E_j.\cos(\delta_j - \delta_s)}{x_j}.$$

3.2.1. Assessing eigenvalues in the conventional droop-based system

By replacing Eq. (4a) in Eq. (33), Eq. (34) is obtained.

$$\frac{dP_j}{dt} = A.\{\omega_{nj} - m_{1j}.P_j - \omega_s\} \tag{34}$$

Therefore, the eigenvalue of a conventional droop based-system is calculated from Eq. (35) below.

$$\lambda = -A.m_{1j} \tag{35}$$

In order for the system to be stable, λ must be negative. This means that m_{1j} must be positive because A is invariably positive.

3.2.2. Assessing eigenvalues in the novel droop-based system

For the novel droop-based system, Eq. (36) is obtained by means of putting Eq. (29) into Eq. (33).

$$\frac{dP_j}{dt} = A.\{\{\omega_{nj} - m_{1j}\left(P_j - P_{0j}\right) - m_{2j}P_j\left(P_j - P_{0j}\right) - \omega_s \tag{36}$$

Then Eq. (37) results from applying Laplace transform to both sides of Eq. (36).

$$A.m_{2j}.S.P_j^2 + \{A.m_{1j} + (1 - A.m_{2j}.P_{0j}).S\}P_j - A.\{\omega_{nj} + m_{1j}.P_{0j} - \omega_s\} = 0 \tag{37}$$

P_j can be written as Eq. (38) assuming $m_{2j} \cong$.

$$P_j = \frac{A.\{\omega_{nj} + m_{1j}.P_{0j} - \omega_s\}}{A.m_{1j} + (1 - A.m_{2j}.P_{0j}).S} \tag{38}$$

Its eigenvalue equals Eq. (39).

$$\lambda = -\frac{A.m_{1j}}{1 - A.m_{2j}.P_{0j}} \tag{39}$$

It is clear that $\frac{m_{1j}}{1 - A.m_{2j}.P_0} >$, A > 0, and $P_0 >$.

It is worth noting that in the conventional droop, $m_{2j} = 0, P_0 = 0$, and $\lambda = -A.m_{1j}$. Thus, the eigenvalue must be more negative in the proposed droop. This gives rise to two modes.

The first mode is $m_{1j} >$ and $(1 - A.m_{2j}P_0) > 0$. In other words, $A.m_{2j}P_0 < 1$. On the other hand, the denominator of the eigenvalue must be smaller than one $((1 - A.m_{2j}P_0) < 1)$. Thus, $0 < m_{2j} < \frac{1}{A.P_0}$.

The second mode is $m_{1j} <$ and $(1 - A.m_{2j}P_0) < 0$. The negative m_{1j} is inconsistent with the condition of the conventional method. Hence, this mode is irrational.

It follows that the conditions $m_{1j} >$ and $0 < m_{2j} < \frac{1}{A.P_0}$ must hold for Eq. (39).

4. Optimization of droop coefficients in the ANLD scheme

Although coefficients m_1 and n_1 are usually determined using Eq. (5) (e.g., [26]), all coefficients (m_1, m_2, n_1, n_2, and n_3) of the proposed scheme are determined using the PSO method in order to obtain the optimal values and desirable conditions of the network. For this purpose, some optimization indices, based on fuzzy logic, are introduced: the most critical eigenvalue index (CEI), the active power index (API), the circulating reactive power index (CRPI), and the voltage index (VI). These indices are further explained below.

4.1. Critical eigenvalue index

First, all eigenvalues of the system are determined. Then an eigenvalue whose real part is the biggest of all the eigenvalues is introduced as the critical eigenvalue (CE). The real part of the CE (RCE) detects the stability margin of the system. Thus, the CEI is defined as in Eq. (40).

$$CEI=\begin{cases} 0 & RCE\leq -0.05 \\ 1+\frac{RCE}{0.05} & RCE> -0.05 \end{cases} \tag{40}$$

This means that if the RCE is smaller than –0.05, the stability status of the system is the best [30]. The larger the RCE is, the worse the stability status will be. This requires the minimization of the CEI. According to Eq. (40), the CEI value is between zero and one.

4.2. Active power index

First, the function API_i is defined as a difference between the output real power of the ith DG unit and average real power (Eq. (41)) [33].

$$API_i=\begin{cases} \frac{DP_i}{0.1P_{av}} & DP_i\leq 0.1P_{av} \\ 1 & 0.1P_{av}<DP_i \end{cases} \tag{41}$$

Here, $DP_i=|P_i-P_{av}|$, P_i is the output real power of the ith DG unit, and P_{av} is the average real power of the network. Then the API represents the status of the generated active power of the network, as given in Eq. (42).

$$API=\frac{1}{NS}\sum_{i=1}^{NS} API_i \tag{42}$$

Here, NS is the number of source buses.

4.3. Circulating reactive power index

This index expresses the normalized circulating reactive power between DGs. When close to zero, the index shows high performance of the system. The CRPI is defined as in Eq. (43).

$$CRPI=\frac{1}{NS.(NS-1)/2}\sum_{s=1}^{NS}\sum_{r=s+1}^{NS} CRP_{sr} \tag{43}$$

Here, CRP_{sr} is expressed as in Eq. (44) and based on the difference between the output reactive power of the DGs [33].

$$CRP_{sr}=\begin{cases} \frac{DQ_{sr}}{0.1Q_{av}} & DQ_{sr}\leq 0.1Q_{av} \\ 1 & 0.1Q_{av}< DQ_{sr} \end{cases} \tag{44}$$

Here, $DQ_{sr}=|Q_s-Q_r|$, Q_s and Q_r are the reactive power of the sth and rth DGs, and Q_{av} is the average reactive power of the network

4.4. Voltage index

When voltage regulation is performed in the n-bus system, then the voltages of the buses will be within the desirable range. The VI shows the status of voltage regulation in the network. In this regard, the function VI_i is defined in terms of the distance between the voltage of the ith bus and the nominal voltage, as Eq. (45) shows.

$$VI_i=\begin{cases} 0 & D_i\leq 0.02 \\ \frac{D_i}{0.08}-0.25 & 0.02 < D_i\leq 0.1 \\ 1 & 0.1<D_i \end{cases} \tag{45}$$

Here, $D_i=|v_i-1|$, and v_i is the ith bus voltage. Now the VI is calculated from Eq. (46), which is the average value of VI_i for all buses of the network. All values are per unit.

$$VI=\frac{1}{n}\sum_{i=1}^{n} VI_i \tag{46}$$

4.5. Global index

Finally, a global index (GI) that is based on the concept of fuzzy logic is formulated. In other words, the GI is defined as the maximum of the values of the individual indices as shown in Eq. (47) below.

$$GI=\max\{CEI, API, CRPI, VI\} \tag{47}$$

Now an optimization problem is introduced as follows.

$$\begin{gathered} \textit{objective function:minimize } GI \\ \textit{subject to:} \\ \begin{array}{ccc} v_{min}\leq v_k\leq v_{max} & , & k=1,2,\ldots,n \\ 0\leq |Q_i|\leq Q_{nominal\ i} & , & i=1,2,\ldots,NS \\ 0\leq P_j\leq P_{nominal\ j} & , & j=1,2,\ldots,NS \end{array} \\ 0\leq m_1 \\ 0\leq m_2\leq \frac{1}{AP_0} \end{gathered}$$

This optimization problem can be solved with different methods. In this research, it is solved via the PSO algorithm [33].

5. Simulation, results, and discussion

The case studies are a 5-bus microgrid (Case I) and a modified 37-bus IEEE microgrid (Case II) [33]. The controller parameters of DG units and the initial conditions of state variables of the PC in both cases are given

in Tables 1 and 2, respectively. To demonstrate the high performance, speed, and precision of the proposed method, a comparison is drawn between this ANLD method (Mode_1) and the three control droop methods presented in the previous literature: the conventional (P-f) and (Q-v) control droops (Mode_2), the (P-f) and (Q-v) droops proposed in [23] (Mode_3), and the (P-f) and (Q-v) droops proposed in [25] (Mode_4). In all four modes, the droop coefficients are optimized by means of the optimization problem introduced in Section 4. The eigenvalues, the stability margin of the system, and the time response of some parameters are computed using the algorithm presented in Section 2.2.

Table 1. The controller parameters of DG units in both cases (per unit, S_{base} = 10 KVA, V_{base} = 4800 V).

ω_c	0.1	r_f	0.1
ω_n	1	L_f	1.35×10^{-3}
K_{iv}	390	C_f	5×10^{-5}
K_{pc}	10.5	r_c	0.03
K_{ic}	16000	L_c	35×10^{-5}
K_{pv}	0.5	F	0.75

Table 2. Initial conditions of state variables of the PC in both cases (per unit).

State variable	P	Q	φ_d	φ_q	γ_d	γ_q	v_{od}	v_{oq}	I_{ld}	I_{lq}	I_{od}	I_{oq}	δ
Initial value	1	0	0	0	0	0	1	0	1	0	1	0	0

5.1. Case I

The one-line diagram of Case I is shown in Figure 5, and Tables 3 and 4 present the details of the lines and loads of Case I, respectively. In this case, three VSI-based DG units share loads at Buses 1, 2, and 5.

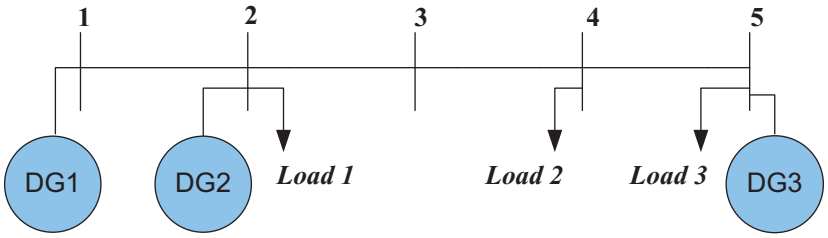

Figure 5. The one-line diagram of 5-bus microgrid (Case I).

Table 3. The line parameters of Case I (Ω).

Line no.	Resistance of lines	Reactance of lines	Shunt admittance of lines
1-2	0.6	0.02	0
2-3	0.5	0.03	0
3-4	2	0.2	0
4-5	3	0.7	0

Table 4. Load parameters of Case I.

Bus no.	Active power (kW)	Reactive power (kVar)
2	65	10
4	35	20
5	10	21

A disturbance happens at 0.8 s, which is a sudden increase in the load at Bus 5. Figure 6 depicts five CEs whose real parts have the biggest values in Mode_1. For all modes, the value of the most critical eigenvalue is given in Table 5. As can be seen, in Mode_1, the stability margin of the system is improved compared to Mode_2 (0.0088 more), Mode_3 (0.0514 more), and Mode_4 (0.0052 more). Table 5 shows also the values of the fuzzy indices defined in Section 4 and the operating points of the system. The PC coefficients of Mode_1 obtained from the optimization problem solution are given in Table 6.

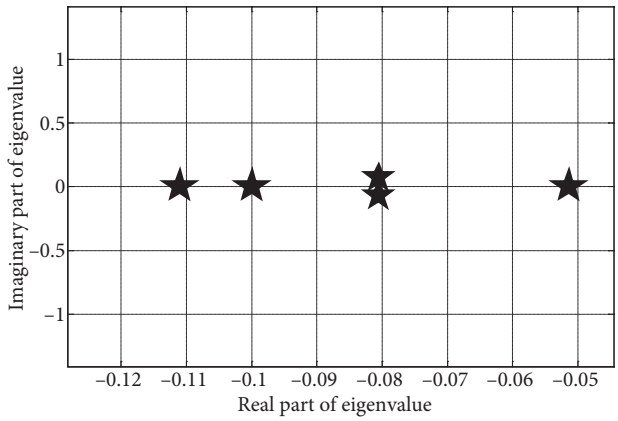

Figure 6. Five CEs of Case I with the biggest values of real parts (Mode_1).

Table 5. The values of the individual and general indices of the optimization problem prior to disturbance for Case I.

INDICES_CASE I	Mode_1	Mode_2	Mode_3	Mode_4
RCE	–0.0514	–0.0426	–3.58E-9	–0.0462
CEI	**0**	0.148	0.99	0.076
P1	2.2588	0.4	0.5369	2.019
P2	1.6134	1.4	1.3422	1.5835
P3	1.1294	2.8	2.6444	1.1537
API	**0.7742**	0.9565	1	**0.6706**
Q1	3.4915	3.0969	3.3029	4.9415
Q2	3.5217	3.4226	3.6552	2.2558
Q3	3.7437	3.3607	2.8493	3.0302
CRPI	**0.4687**	0.659	1	1
V1	0.9906	0.9479	0.9446	0.9659
V2	0.99	0.9478	0.9444	0.9653
V3	0.9893	0.9476	0.9441	0.9647
V4	0.9867	0.9467	0.9431	0.9622
V5	0.9864	0.9487	0.9449	0.9618
VI	**0**	0.403	0.447	0.2
GI	**0.7742**	0.9565	1	1

Given the disturbance at 0.8 s, the voltage values of the buses are within the desirable range in Mode_1. For this case, Figure 7 portrays the output voltage of DG units in all modes. The VI and CRPI values of Mode_1 are obtained as 0 and 0.4687, respectively, which are the best values.

Although Mode_4 gives an API of 0.6706, which is less than the API of Mode_1 (0.7742), it cannot be effective on other parameters. Finally, as can be concluded from Table 5, the GI of Mode_1 has the minimum

value (the best value) in comparison with the other modes. Figures 8 and 9 show the output reactive and active power sharing of DG units, respectively. The frequency is kept at the nominal value, according to Figure 10. Hence, the results and simulations indicate the high performance of the proposed scheme in the small-signal stability of the system, accurate load sharing, and voltage and frequency regulation despite load or generation surge.

Table 6. Droop coefficients of Case I in Mode$_1$.

	DG1	DG2	DG3
m_1	0.150×10^{-8}	0.210×10^{-8}	0.300×10^{-8}
m_2	0.126×10^{-8}	0.619×10^{-7}	0.115×10^{-7}
n_1	$0.\ 8149\times10^{-2}$	$0.\ 8163\times10^{-2}$	$0.\ 8146\times10^{-2}$
n_2	$0.\ 91\times 10^{-2}$	0.91×10^{-2}	0.914×10^{-2}
n_3	$0.\ 91\times 10^{-2}$	0.91×10^{-2}	0.0914×10^{-2}
$Q_0(pu)$	0	0	0
$P_0(pu)$	0	0	0
$V_n(pu)$	1.050064	1.050045	1.0501124

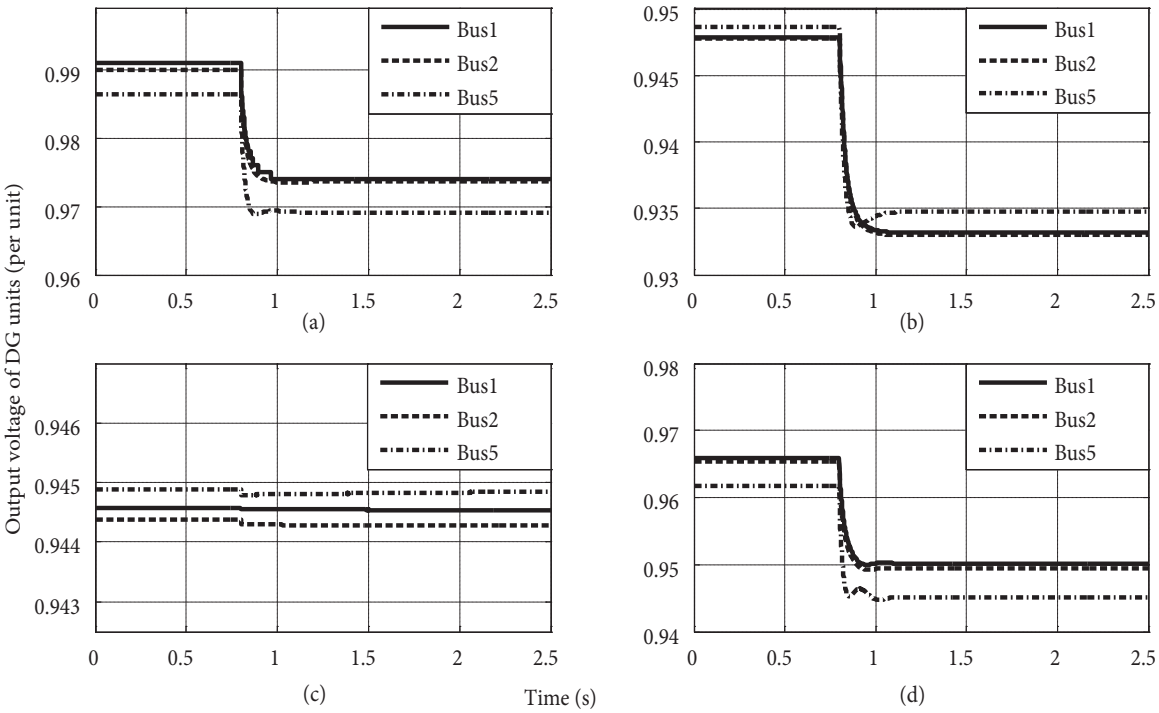

Figure 7. The output voltage of DG units of Case I: (a) Mode$_1$, (b) Mode$_2$, (c) Mode$_3$, (d) Mode$_4$.

5.2. Case II

Figure 11 displays the one-line diagram of Case II. The values of the lines and loads of Case II are given in Tables 7 and 8, respectively. In this case, there are three VSI-based DG units at Buses 10, 15, and 17. At 0.8 s, the load of Bus 5 increases.

Table 7. Line parameters of Case II (Ω).

Line no.	Resistance of lines	Reactance of lines	Shunt admittance of lines
1-2	0.2978	0.2049	0
2-3	0.1545	0.1063	0
3-4	0.2125	0.1462	0
4-5	0.4420	0.2245	0
5-6	0.1473	0.0748	0
6-7	0.2357	0.1197	0
7-8	0.2357	0.1197	0
8-9	0.4125	0.2095	0
9-10	0.4715	0.2394	0
10-11	0.2947	0.1496	0
11-12	0.2947	0.1496	0
12-13	0.2947	0.1496	0
3-14	0.2591	0.1347	0
14-15	0.3831	0.1945	0
15-28	0.0589	0.0299	0
28-29	0.3831	0.1945	0
15-16	0.5893	0.2993	0
16-33	0.4420	0.2245	0
33-34	0.2063	0.1047	0
16-30	0.6777	0.3442	0
30-31	0.5599	0.2843	0
30-32	0.0884	0.0449	0
3-17	0.2947	0.1496	0
17-18	0.2357	0.1197	0
17-27	0.1768	0.0898	0
4-19	0.1768	0.0898	0
19-20	0.2063	0.1047	0
20-21	0.2063	0.1047	0
20-37	0.1473	0.0748	0
6-22	0.4420	0.2245	0
6-23	0.0001	0.0001	0
7-24	0.2357	0.1197	0
9-25	0.3831	0.1945	0
25-36	0.9429	0.4788	0
25-35	0.1473	0.0748	0
12-26	0.1473	0.0748	0

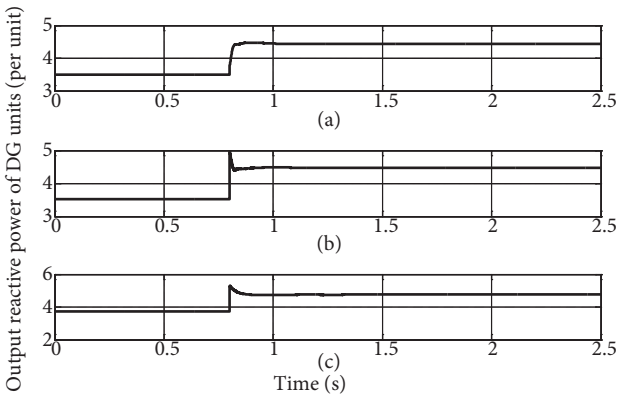

Figure 8. The output reactive power sharing of DG units of Case I (Mode$_1$): (a) DG1, (b) DG2, (c) DG3.

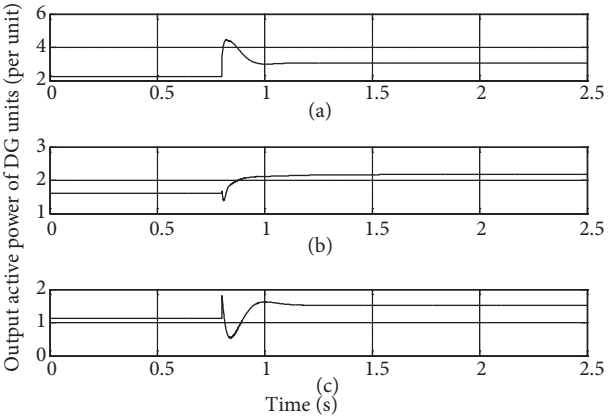

Figure 9. The output active power sharing of DG units of Case I (Mode$_1$): (a) DG1, (b) DG2, (c) DG3.

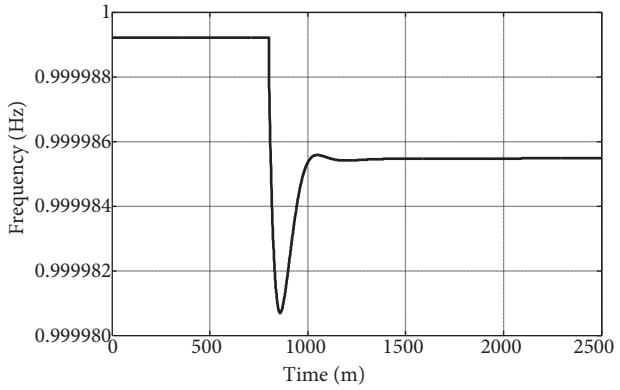

Figure 10. The system frequency of Case I (Mode$_1$).

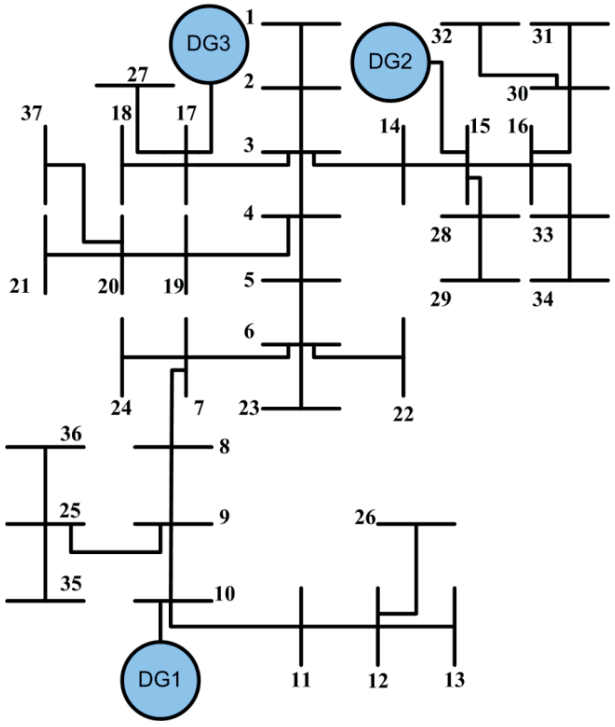

Figure 11. The one-line diagram of modified 37-bus IEEE microgrid (Case II).

In the ANLD scheme, to analyze the power system, the algebraic and dynamic equations of the microgrid are carefully formulated and then used for computing the operating point and time response of system variables. The obtained power controller coefficients can be seen in Table 9.

Table 10 expresses the values of the individual and general indices obtained from the optimization problem and also the operating point and RCE of the system for all modes. The five CEs of Case II with the biggest values of their real parts are demonstrated in Figure 12. It can be seen that the system stability of the microgrid in Mode$_1$ is 0.0435, which is comparable to the system stability in Mode$_2$ (0.0339) and Mode$_4$ (0.0146) and

superior to that in Mode_3 (3.7E-7). It is also clear from Table 10 that the VI value obtained in Mode_1 is the best value. In other words, it is less than the values in Mode_2 (0.5405 less), Mode_3 (0.5373 less), and Mode_4 (0.7507 less). For all modes, Figure 13 depicts the output voltage curve of the source buses. The results of simulating reactive and active power sharing are demonstrated in Figures 14 and 15, respectively. Unlike the other four methods, using the proposed scheme, reactive power is shared properly, causing the CRPI to decrease to 0.8218.

Table 8. Load parameters of Case II.

Bus no.	Active power (kW)	Reactive power (kVar)
2	210	105
5	28	14
8	28	14
9	14	7
10	46	23
11	42	21
13	14	7
14	28	14
16	28	14
18	31	15
19	14	7
20	14	7
21	14	70
22	28	14
24	14	7
26	28	14
27	28	14
28	12	6
29	28	14
31	14	7
32	53	26
34	14	7
35	28	14
36	14	7
37	42	21

Table 9. Droop coefficients of Case II in Mode_1.

	DG1	DG2	DG3
m_1	0.300×10^{-8}	0.300×10^{-8}	0.380×10^{-8}
m_2	0.100×10^{-9}	0.100×10^{-9}	0.100×10^{-9}
n_1	0.824×10^{-8}	0.736×10^{-8}	0.968×10^{-8}
n_2	$0.\ 914931\times10^{-2}$	$0.\ 914931\times10^{-2}$	$0.\ 914931\times10^{-2}$
n_3	$0.\ 914931\times10^{-2}$	$0.\ 914931\times10^{-2}$	$0.\ 0914931\times10^{-2}$
$Q_0(pu)$	8	5	7
$P_0(pu)$	0	0	0
$V_n(pu)$	1.1006419	1.1004584	1.153112

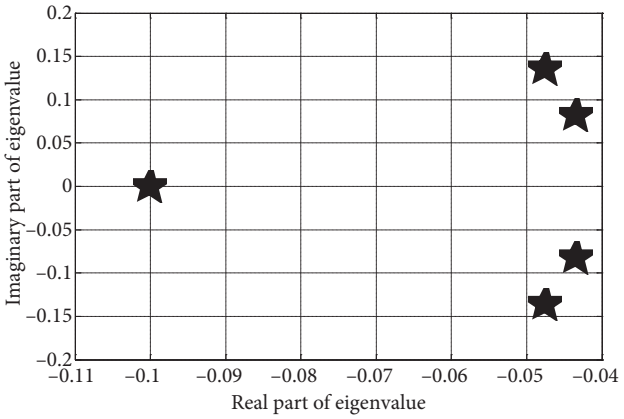

Figure 12. Five CEs of Case II with the biggest values of real parts (Mode_1).

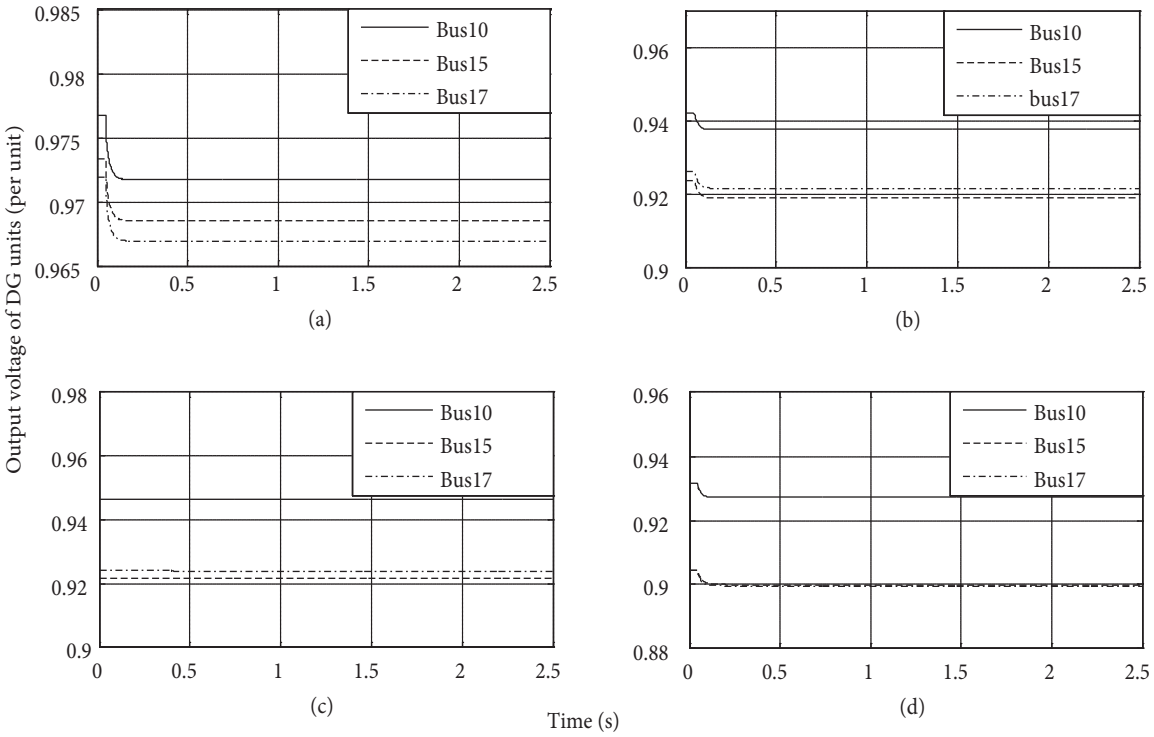

Figure 13. The output voltage of DG units of Case II: (a) Mode_1, (b) Mode_2, (c) Mode_3, (d) Mode_4.

Although Mode_2 gives a better value for the API than Mode_1 does, it cannot produce better results for the other indices (CEI, CRPI, VI, and GI) than Mode^1 does. On the other hand, the significant superiority of Mode_1 comes with the minimum value of GI and the frequency stability shown in Figure 16. According to the obtained results, the conclusion drawn about Case II is similar to the conclusion for Case I.

In conclusion, the ANLD method preserves the small-signal stability of the system, distributes the loads among the inverters without using the communication links, and maintains the voltage and frequency of the network at nominal values. This scheme can be successfully run on complicated microgrids as in Case II. However, in most previous studies, case test configurations were simple. The results prove the superiority of the proposed scheme over other methods proposed in the literature.

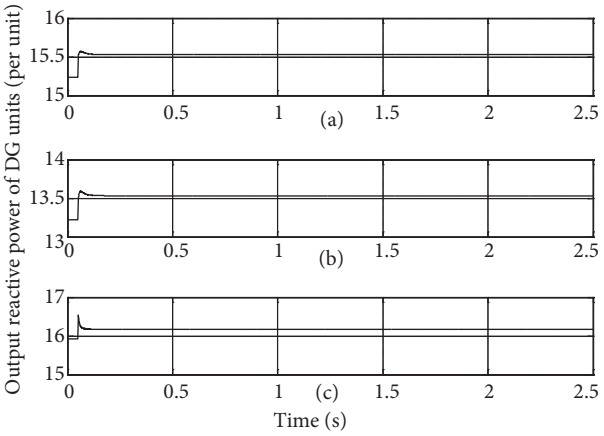

Figure 14. The output reactive power sharing of DG units of Case II (Mode$_1$): (a) DG1, (b) DG2, (c) DG3.

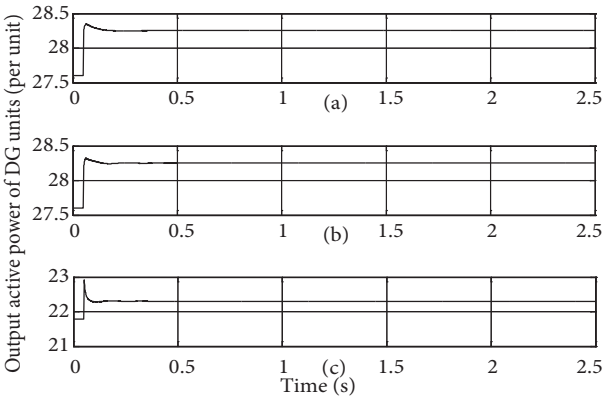

Figure 15. The output active power sharing of DG units of Case II (Mode$_1$): (a) DG1, (b) DG2, (c) DG3.

Table 10. The values of the individual and general indices of the optimization problem prior to disturbance for Case II.

INDICES_CASE II	Mode$_1$	Mode$_2$	Mode$_3$	Mode$_4$
RCE	–0.0435	–0.0339	–3.7E-7	–0.0146
CEI	**0.13**	0.322	0.99	0.708
P1	27.6	37.0093	43.374	45.3702
P2	27.6	9.964	8.4339	15.1234
P3	21.7895	23.5514	18.9763	7.8224
Pav	25.66	23.51	23.59	22.772
API	**0.837**	**0.6607**	1	1
Q1	15.2339	14.4897	14.3013	15.1141
Q2	13.2214	16.6805	16.8648	11.414
Q3	15.9241	9.4657	9.6065	12.8115
Qav	14.8298	13.5453	13.59	13.1132
CRPI	**0.8218**	1	1	1
VI	**0.124**	0.6645	0.6613	0.8747
GI	**0.837**	1	1	1

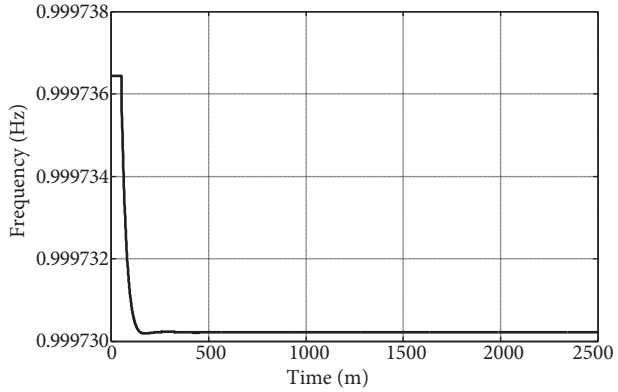

Figure 16. The system frequency of Case II (Mode$_1$).

6. Conclusion

This research proposes a decentralized control method, voltage and frequency adaptive nonlinear droop, for controlling power sharing in autonomous VSI-based microgrids. This scheme increases the network stability margin, optimally and appropriately shares the loads, regulates the voltage, and maintains frequency stability without using communication links. Unlike the conventional power-flow method, the proposed method models and solves the power-flow equations of microgrids without the slack bus and the PV buses. When the demand changes, the output voltage of DG units and the frequency of the network vary depending on reactive and active power, respectively. The droop coefficients are obtained using an optimization problem where a global index is defined as the objective function based on four individual indices. The results demonstrate that the ANLD scheme has a better performance compared with other droop schemes. This algorithm can also be coded in the m-file of MATLAB, which is a perfect easy-to-use and high-speed software application compared to PSCAD and MATLAB/simulation.

Nomenclature

Abbreviations

VSI	Voltage source inverter
DG	Distributed generation
ANLD	Adaptive nonlinear droop
Q/V	Reactive power/voltage
P/f	Active power/frequency
PC	Power controller
VC	Voltage controller
CC	Current controller
FS	Filtering system

Indices

CEI	Critical eigenvalue index
CRPI	Circulating reactive power index
VI	Voltage index
API	Active power index
GI	General index
RCE	Real part of critical eigenvalue

Parameters and variables

ϑ_i	The difference in angle between the reference frame and the ith frame
f_{dqi}	A parameter in the rotating frame of the ith DG unit
f_{DQ}	A parameter in the rotating reference frame
TMi	Transfer matrix of the ith DG unit
e_{od}, e_{oq}	The direct and quadratic component of measured output voltage of the DG unit
e^*_{od}, e^*_{oq}	The reference magnitude of the direct and quadratic component of the output voltage of the DG unit
i_{od}, i_{oq}	The direct and quadratic component of measured output current of the DG unit
ω_c	The cut-off frequency of the low-pass filter
$\tilde{p}, \tilde{q}$	The instantaneous active and reactive power of the DG unit
P, Q	The average active and reactive power of the DG unit
ω	The rotating frequency of the nonreference DG unit
ω_n	The system nominal frequency
ω_{com}	The rotating frequency of the reference DG unit
m_i, n_i	The coefficients of (P/f) and (Q/V) droops
I_j, θ_j	The output current amplitude and phase of the jth DG
E_j	The output voltage amplitude of the jth DG unit
δ_j	The output voltage phase of the jth DG unit
Z_j	The impedance of the jth line
r_j, x_j	The resistance and reactance of the jth line
$\lvert V_j\rvert, \alpha_j$	The output voltage amplitude and phase of the jth bus
S_j	The power generated by the jth DG unit
$\lvert E_{0j}\rvert$	The nominal magnitude of the output voltage of the DG unit
P_{0j}, Q_{0j}	The nominal output active and reactive power of the DG unit
λ	The eigenvalue of the DG unit
F, k_{pv}, k_{iv}	The control parameters of the VC
φ_d, φ_q	The errors of the PI in the VC
k_{pc}, k_{ic}	The control parameters of the CC
C_f, L_f	The capacitance and inductance of the LC filter in the FS
r_{c0}, L_c	The resistance and inductance of the coupling impedance in the FS
γ_d, γ_q	The errors of the PI in the CC
x	The dynamic-state variable of the

	microgrid
y	The algebraic-state variable of the microgrid
z	The miscellaneous parameter of the microgrid
$H(x,y,z)$	The dynamic equation vector of the microgrid
$E(x,y,z)$	The algebraic equation vector of the microgrid
NS	The number of source buses
n	The number of buses in the microgrid
D_i	The difference between the ith bus voltage and the nominal voltage
DPi	The difference between the output active power of the ith DG unit and the average active power of the microgrid
DQi	The difference between the output reactive power of the ith DG unit and the average reactive power of the microgrid
A	The system state matrix
J	The system Jacobean matrix

References

[1] Katiraei F, Iravani R, Hatziargyriou N, Dimeas A. Microgrids management. IEEE Power Energy M 2008; 6: 54–65.

[2] Lasseter RH, Paigi P. Microgrid: a conceptual solution. In: 35th Power Electronics Specialists Conference; 2004. New York, NY, USA: IEEE. pp. 20–25.

[3] Katiraei F, Iravani MR. Power management strategies for a microgrid with multiple distributed generation units. IEEE T Power Syst 2006; 21: 1821–1831.

[4] Dragicevic T, Guerrero JM, Vasquez JC, Skrlec D. Supervisory control of an adaptive-droop regulated DC microgrid with battery management capability. IEEE T Power Electr 2014; 29: 695–706.

[5] Tsikalakis AG, Hatziargyriou ND. Centralized control for optimizing microgrids operation. IEEE T Energy Conver 2008; 23: 241–248.

[6] Soultanis NL, Papathanasiou SA, Hatziargyriou ND. A stability algorithm for the dynamic analysis of inverter dominated unbalanced LV microgrids. IEEE T Power Syst 2007; 22: 294–304.

[7] Majumder R, Chaudhuri B, Ghosh A, Majumber R, Ledwich G, Zare F. Improvement of stability and load sharing in an autonomous microgrid using supplementary droop control loop. IEEE T Power Syst 2010; 25: 796–808.

[8] De D, Ramanarayanan V. Decentralized parallel operation of inverters sharing unbalanced and nonlinear loads. IEEE T Power Electr 2010; 25: 3015–3025.

[9] Prodanovic M, Green T, Mansir H. A survey of control methods for parallel three-phase inverters connection. In: Instrument Electronics Engineering Conference; 2000. New York, NY, USA: IEEE. pp. 472–477.

[10] Chen J, Chu C. Combination voltage-controlled and current controlled PWM inverters for UPS parallel operation. IEEE T Power Electr 1995; 10: 547–558.

[11] Pecas Lopes JA, Moreira CL, Madureira AG. Defining control strategies for microgrids islanded operation. IEEE T Power Syst 2006; 21: 916–924.

[12] Pogaku N, Prodanovic M, Green TC. Modeling, analysis and testing of autonomous operation of an inverter-based microgrid. IEEE T Power Electr 2007; 22: 613–625.

[13] Chandorkar MC, Divan DM, Adapa R. Control of parallel connected inverters in standalone AC supply systems. IEEE T Ind Appl 1993; 29: 136–143.

[14] Marwali MN, Jung JW, Keyhani A. Control of distributed generation systems-part II: load sharing control. IEEE T Power Electr 2004; 19: 1551–1561.

[15] Gao F, Iravani MR. A control strategy for a distributed generation unit in grid-connected and autonomous modes of operation. IEEE T Power Deliver 2008; 23: 850–859.

[16] Coelho EAA, Cortizo PCC, Garcia PFD. Small-signal stability for parallel-connected inverters in stand-alone AC supply systems. IEEE T Ind Appl 2002; 38: 533–542.

[17] Majumder R, Ghosh A, Ledwich G, Zare F. Load sharing and power quality enhanced operation of a distributed microgrid. IET Renew Power Gen 2009; 3: 109–119.

[18] Sao CK, Lehn PW. Control and power management of converter fed microgrids. IEEE T Power Syst 2008; 23: 1088–1098.

[19] Engler A. Applicability of droops in low voltage grids. DER J 2005; 1: 1–5.

[20] Yu X, Khambadkone AM, Wang H, Terence STS. Control of parallel-connected power converters for low-voltage microgrid—Part I: a hybrid control architecture. IEEE T Power Electr 2010; 25: 2962–2970.

[21] Gao F, Iravani MR. A control strategy for a distributed generation unit in grid-connected and autonomous modes of operation. IEEE T Power Deliver 2008; 23: 850–859.

[22] Vasquez JC, Guerrero JM, Luna A, Rodriguez P, Teodorescu R. Adaptive droop control applied to voltage-source inverters operating in grid-connected and islanded modes. IEEE T Ind Electron 2009; 56: 4088–4096.

[23] Sao CK, Lehn PW. Autonomous load sharing of voltage source converters. IEEE T Power Deliver 2005; 20: 1009–1016.

[24] Savaghebi M, Jalilian A, Vasquez JC, Guerrero JM. Secondary control scheme for voltage unbalance compensation in an islanded droop-controlled microgrid. IEEE T Smart Grid 2012; 3: 797–807.

[25] Yari M, El-Saadany EF. Adaptive decentralized droop controller to preserve power sharing stability of paralleled inverters in distributed generation microgrids. IEEE T Power Electr 2008; 23: 2806–2816.

[26] Rokrok E, Golshan MEH. Adaptive voltage droop scheme for voltage source converters in an islanded multi bus microgrid. IET Gener Transm Dis 2010; 4: 562–578.

[27] Bollen MHJ, Sannino A. Voltage control with inverter-based distributed generation. IEEE T Power Deliver 2005; 20: 519–520.

[28] Cardell J, Ilić M. Maintaining stability with distributed generation in a restructured industry. In: Power Engineering Society General Meeting; 2004 New York, NY, USA: IEEE. pp. 2142–2149.

[29] Kundur P, Balu NJ. Power System Stability and Control. New York, NY, USA: McGraw-Hill, 1998.

[30] Tinney WF, Hart CE. Power flow solution by Newton's method. IEEE T Power Ap Syst 1967; 86: 1449–1460.

[31] Brenan KE, Campbell SL, Petzold L. Numerical Solution of Initial-Value Problems in Differential-Algebraic Equations. Philadelphia, PA, USA: SIAM, 1995.

[32] Díaz G, González-Morán C, Gómez-Aleixandre J, Diez A. Complex-valued state matrices for simple representation of large autonomous microgrids supplied by PQ and Vf generation. IEEE T Power Syst 2009; 24: 1720–1730.

[33] Hasanpor Divshali P, Hosseinian SH, Abedi M, Alimardani A. Small-signal stability and load-sharing improvement of autonomous microgrids using auxiliary loop. Electr Pow Compo Sys 2012; 40: 648–671.